Experimental study of Cr incorporation in pargasite

Claire-Isabelle Fialips-Guédon, Jean-Louis Robert, François Delbove

Experimental study of Cr incorporation in pargasite

CLAIRE-ISABELLE FIALIPS-GUÉDON,[1] JEAN-LOUIS ROBERT,[2] AND FRANÇOIS DELBOVE[2]

[1]Thermochemistry Facility, Department of Chemical Engineering and Materials Science, University of California at Davis, One Shields Avenue, Davis, California 95616, U.S.A.
[2]Centre de Recherche sur la Synthèse et la Chimie des Minéraux, and FR 09, CNRS, 1A rue de la Férollerie, 45071 Orléans Cedex 2, France

ABSTRACT

Pargasite compositions corresponding to the nominal structural formula $NaCa_2$ $(Mg_4Al_{1-x}Cr_x)(Si_6Al_2)O_{22}(OH)_2$, with $0 \leq x \leq 1$, were investigated at 900 °C and 3 and 20 kbar P_{H_2O}. The aims of this work were to determine the extent of the solid solution, i.e., the maximum x value, as a function of experimental conditions, and to characterize the M^{3+} (Al^{3+} and/or Cr^{3+}) distribution over the M sites. A first series of experiments at 900 °C and 3 kbar showed the presence of large amounts of Cr^{6+} as sodium chromate (Na_2CrO_4) and dichromate ($Na_2Cr_2O_7$) in the final fluid phase, which promotes the extraction of Cr from the bulk solid (up to 45 mol%). The oxidizing agent was the oxygen from water, liberated by diffusion of hydrogen from water through the Pt tube wall. To prevent this oxidation, a new double-chamber tube was designed, one chamber containing powdered metallic Cr to trap the excess of oxygen and the second chamber initially containing the starting gel and water. Using this tube, (chromium)-pargasites were produced with a maximum Cr content around 0.43 apfu from EMP analyses (based on 23 O atoms), close to the maximum Cr solubility observed in naturally occurring pargasites. In FTIR spectra of Cr-free pargasite, two intense OH-stretching bands are observed at 3714 and 3681 cm^{-1}, corresponding to OH groups adjacent to Mg_3 and to Mg_2Al, respectively, and pointing toward a filled A-site. A third band is observed at 3656 cm^{-1}, which can be assigned to OH groups pointing toward vacant A-sites. Along the Al-Cr pargasite join, significant modifications are observed in the OH-stretching region: a new band appears at 3660 cm^{-1}, which can be assigned to OH groups adjacent to Mg_2Cr, and pointing toward a filled A-site. Its relative intensity increases regularly with the Cr content, showing that Cr^{3+} enters M site(s) adjacent to an OH group. Combining EMP and FTIR data, we conclude that up to 0.27 Cr per formula unit occupies the M3 site. However, these are more octahedral trivalent cations than expected, and these are balanced by lower tetrahedral Al and lower occupancies of the A and M4 sites. This charge arrangement, with important deviations from ideal stoichiometry, is apparently the only stable one under the conditions applied. Results were confirmed at 900 °C and 20 kbar P_{H_2O}, indicating that increasing pressure does not affect Cr solubility in pargasite.

INTRODUCTION

Pargasite is a monoclinic amphibole end-member with ideal formula $NaCa_2Mg_4AlSi_6Al_2O_{22}(OH)_2$. The tetrahedral double-chain is composed of T1 and T2 sites. T1 sites accommodate Si and Al whereas T2 sites accommodate mainly Si. The octahedral strip is composed of two M1, two M2, and one M3 site per formula unit. The M1 and M3 sites are adjacent to four O atoms and two hydroxyl groups, in cis and trans positions, respectively, whereas the M2 site is adjacent to six O atoms. In the present study, these octahedral sites can accommodate Mg^{2+}, Al^{3+}, and Cr^{3+}. The M4 site is a wide, anti-prismatic pseudo-cubic cavity that can accommodate mainly Na^+ and Ca^{2+} but also Mg^{2+}. In pargasite, the A-site is mostly occupied by Na^+, but it can be also partly vacant.

Pargasites are encountered from the Earth's upper mantle to the crust (Deer et al. 1992). Their origin in mantle rocks is controversial: some authors consider pargasites to be primary phases, stable at the liquidus of basic melts, whereas other ones consider these amphiboles to be the result of metasomatic pro-

cesses affecting the upper mantle (Veblen and Ribbe 1982). Chromium-rich pargasites commonly occur as inclusions in ophiolitic complexes and in chromitites from mafic-ultramafic layered complexes (Johan et al. 1983). The maximum reported chromium content of pargasite seems to be around 3.5 wt% of Cr_2O_3, i.e., close to 0.5 Cr atom per formula unit (apfu) (Johan et al. 1983). For example, the average structural formula, based on several tens of analyses of (chromium)-pargasite inclusions in chromites from the Oman ophiolitic complex, is: $(Na_{0.57}K_{0.03})(Ca_{1.57}Mg_{0.43})(Mg_{3.91}Fe^{2+}_{0.30}Cr_{0.42}Al_{0.22}Ti_{0.17})$ $(Si_{6.38}Al_{1.62})O_{22}(OH)_2$ (Augé, personal communication, 1996). These amphiboles, included in chromites, are commonly associated with phases of the high-temperature decomposition paragenesis of pargasite: Al-rich diopside, forsterite, nepheline, spinel (the chromite itself), anorthite, plus Na-rich trioctahedral micas (Johan et al. 1983).

Experiments were performed under hydrothermal conditions along the $NaCa_2(Mg_4Al)(Si_6Al_2)O_{22}(OH)_2$-$NaCa_2(Mg_4Cr)(Si_6Al_2)O_{22}(OH)_2$ join, at 900 °C and 3 and 20 kbar P_{H_2O}, using different fluid compositions. The aims of the study were to analyze the Cr solubility in pargasites, and to understand the incorporation mechanism of Cr into the am-

*E-mail: cifialips@ucdavis.edu

phibole structure and its distribution between the different sites. The crystal-chemical approach is based on X-ray diffraction (XRD) data, and Fourier transform infrared absorption spectrometry (FTIR) measurements in the OH-stretching region. The valence state of Cr in experimental systems was also considered.

MATERIALS AND METHODS

Six gels of different compositions were prepared according to the gelling method of Hamilton and Henderson (1968), using high-grade Na_2CO_3, $CaCO_3$, and Cr^0 (transformed to Na, Ca, and Cr^{3+} nitrates by dissolution in HNO_3), titrated. Mg and Al nitrate solutions, and tetraethylorthosilicate (TEOS) as starting reagents (Guédon 1996). Samples were synthesized along the theoretical $NaCa_2(Mg_4Al)(Si_6Al_2)$ $O_{22}(OH)_2$-$NaCa_2(Mg_4Cr)(Si_6Al_2)O_{22}(OH)_2$ join, by replacing $^{[6]}Al$ with $^{[6]}Cr$ in the starting gel, with nominal compositions measured by the atomic fraction of Cr $[0 \leq X_{Cr} = {}^{[6]}Cr / {}^{[6]}(Cr + Al) \leq 1]$.

Two series of experiments were performed at 900 °C and 3 kbar, for 3 days in an internally heated pressure vessel, using Ar as the pressure medium. These conditions were chosen according to previous experimental studies on pargasite (Della Ventura et al. 1999).

For the first series of syntheses, 160–190 mg of starting gel and 24–29 µL of solution (15 wt%) were introduced into Pt tubes. The solution used was distilled water for the most part, but three experiments were performed using increasingly concentrated NaCl solutions (1–4 M).

For the second series of syntheses, a double-chamber tube was designed, one chamber initially containing 120–240 mg of starting gel and 18–36 µL of distilled water (15 wt%), and the second chamber containing 300 mg of powdered metallic Cr. The two chambers were partitioned using Pt foils.

The Pt tubes were sealed by arc welding, and placed into a stainless-steel sample holder, inside the pressure vessel. The temperature was measured by two Chromel-Alumel thermocouples located within the sample holder, in contact with the Pt tubes. The uncertainty on temperature measurements is lower than ±10 °C, and no temperature gradient greater than 3 °C was observed along the tubes. The pressure was measured with a Bourdon manometer, with an accuracy of ±50 bars.

One synthesis was performed at 900 °C and 20 kbar for 7 hours in a piston-cylinder apparatus, using 114 mg of starting gel and 20 µL of distilled water (17.5 wt%) placed into a nonsealed Pt tube.

Run product solid and fluid phases were separated by washing and filtering.

ANALYTICAL TECHNIQUES

X-ray diffraction

All products were examined by XRD, by reflection mode on powder preparations, using a Siemens diffractometer equipped with a Fe-filtered Co$K\alpha$ radiation (40 kV, 20 mA), combined with a SOCABIM system (DACO-MP) for numerical data acquisition. Diffraction patterns were recorded by step scanning, using a step interval of 0.025° 2θ and a counting time of 5 s per step. Unit-cell parameters (a, b, c, and β) of synthesized pargasites were refined with the "Least-Squares Unit-Cell Refinement" Program of Appleman and Evans (1973), as modified by Garvey (1987). A set of at least 30 unambiguously indexed peaks was used for pargasites corresponding to low nominal X_{Cr} values (≤0.6). For higher bulk Cr contents, the increasing proportion of pyroxene reduced to about 20 the number of unambiguous diffraction lines used for the refinement of the amphibole cell dimensions.

Fourier transform infrared absorption spectrometry

Infrared spectra were recorded in the 3800–3500 cm^{-1} range, with a 2 cm^{-1} nominal resolution, on a Nicolet 710 spectrometer swept by a permanent dry air flow. The scanning condition was 400 scans for both the background and the samples. Spectra were obtained by transmission mode from KBr pressed pellets. Pellets were prepared by homogeneous mixing 7–8 mg of dry sample with 150 mg of KBr.

Infrared spectra were decomposed in symmetrical Gaussians with the SPC program (Roux and Volfinger 1996); the reason of the use of symmetrical Gaussians was discussed previously by Strens (1974) and Papin et al. (1997).

Quantitative analysis of the cation site populations adjacent to OH groups from FTIR data needs the knowledge of molar extinction coefficients. Absolute values of these extinction coefficients are not available for most cationic environments; however, we know that they remain constant when the wavenumber changes, even when transition elements are involved, provided that the second- and third-neighbor cationic environments remain unchanged in the amphibole structure (Della Ventura et al. 1996, 1997).

Electron microprobe

A CAMECA SX50 electron microprobe was used to analyze the synthetic pargasites and to derive their structural formula. The analytical conditions were: 6 nA, 15 kV, and 10 s per analysis. The standards used were albite for Si and Na, corundum for Al, andradite for Ca, eskolaite for Cr, and forsterite for Mg. The amphibole grains were generally too small for microprobe analysis, but those produced from the bulk nominal compositions corresponding to $X_{Cr} = 0.6$ and $X_{Cr} = 1$ (up to 10 µm) allowed good quality measurements. For each sample, at least 20 analyses were performed. Only those analyses giving total oxides >90 wt% were considered reliable and were averaged.

Absorption spectrophotometry

Solutions in equilibrium with the final solids were analyzed by spectrophotometry to determine the valence state of Cr and its concentration in solution. The Zeiss Aspect V2.02 apparatus used is a single-beam spectrophotometer. The acquisition wavenumber range was 250–650 nm, with an integration time of 84 s. The standards used were pH-buffered sodium dichromate solutions ($Na_2Cr_2O_7 \cdot 2H_2O$, pH = 10.01).

Atomic absorption spectrometry

Atomic absorption spectrometry (AAS) allowed the quantification of the Na content in the residual solutions. The spec-

trometer used is a GBC 905 AA with an air-acetylene flame. The wavelength used was 589 nm (sodium).

EXPERIMENTAL RESULTS AND DISCUSSION

Synthesis conditions and parageneses obtained are given in Table 1. Pargasite was formed as a major phase whatever the conditions of synthesis were. However, pargasite was always associated with diopside. The amount of diopside was always minor but increased with the bulk X_{Cr} value.

Experiments without Cr metal

For nominal $X_{Cr} = 0.2$–1.0, solid phases were green, indicating the presence of Cr^{3+}, whereas solutions were orange-yellow, suggesting the presence of Cr^{6+}.

AS and AAS. Analyses of the orange-yellow fluid phases revealed the presence of large amounts of Cr^{6+} and Na^+, as sodium chromate and dichromate (Na_2CrO_4 and $Na_2Cr_2O_7$). Up to 45% of the initial Cr, and 30% of the initial Na, remained in the fluid phase (Table 2). The proportion of the two Cr-bearing species in solution was variable as reflected by the Na/Cr ratio (Table 2).

The solubilization of Cr as sodium chromate and dichromate may result from two possible mechanisms:

(1) A dismutation reaction, $2\ Cr^{3+} \rightarrow Cr^{6+} + Cr^0$. Sodium chromate and dichromate would be formed by association of Cr^{6+} and Na^+ extracted from the gel. In this hypothesis, the expected amount of Cr^0 should be equal to the amount of Cr^{6+}, and could therefore reach up to 45 mol% of the initial Cr content of the system (Table 2). Chromium could be present either as pure metal in the run products, or forming a Pt-Cr alloy with the tube wall. No Cr^0 was observed in run products, and EMP analyses of the Pt tubes after runs did not show any detectable Cr in the Pt. Therefore, this hypothesis was ruled out.

(2) Decomposition of a fraction of water, $H_2O \leftrightarrow H_2 + 1/2O_2$. Hydrogen diffuses through the Pt tubes, and the system is progressively enriched in oxygen; oxidation of Cr^{3+} to Cr^{6+} produces sodium chromate and dichromate in solution (Fig. 1a).

XRD. Unit-cell dimensions of the pargasites are given in Table 3 as a function of the Cr content of the starting gel. The a edge and the β angle decrease slightly but there is no clear change in the b, c, and V dimensions within the limits of precision, indicating that very little Cr has entered the amphibole

structure. The decrease of a as X_{Cr} increases reflects an increase of the proportion of vacant A-sites resulting from the progressive release of sodium as sodium chromate and dichromate to the fluid phase. As a matter of fact, when an A-site is empty, there is no longer repulsion between the hydroxyl proton H^+ and sodium Na^+, which results in a flattening of the structure along a^* (Hawthorne et al. 1997).

Experiments with Cr metal

The experimental setup used in the first series of experiments was not satisfactory because it produces large amounts of Cr^{6+}, which results in a very low Cr incorporation into the pargasite structure. Therefore, to increase Cr incorporation into the amphibole structure, the double-chamber tube setup was developed to prevent Cr^{3+} oxidation by trapping the excess oxygen within the tube with Cr metal (Fig. 1b).

At the end of syntheses, the first Pt tube chamber, initially containing gel and distilled water, contained dark-green solid phases, indicating the presence of Cr^{3+}, and uncolored solutions, reflecting the absence of Cr^{6+}. The second chamber, initially loaded with Cr metal, contained a dark-green agglomerate, indicating the presence of Cr^{3+}.

AA. No chromium (Cr^{6+}) was detected in the final fluids; therefore, no oxidation of $Cr^{3+} \rightarrow Cr^{6+}$ occurred.

XRD. For low bulk X_{Cr} values ($X_{Cr} = 0.2$ and 0.4), the yield of experiments was close to 100% pargasite in the first chamber, with only a minor amount of diopside. For higher bulk X_{Cr} values, the amount of pyroxene was significant but the amphibole remained the major phase (Table 1).

The solid phase contained in the second chamber was eskolaite (Table 1). Thus, the oxygen resulting from water decomposition was trapped by Cr^0, which was oxidized to Cr^{3+} (Fig. 1b).

Unit-cell dimensions of pargasites crystallized with the double-chamber tube setup are given in Table 4 as a function of X_{Cr}. The a cell parameter remains constant in this sample series. Thus, either the A sites are always full or pargasite always contains the same proportion of vacant A sites. The c and β dimensions remain constant within experimental uncertainties but b increases. The increase of the b edge reflects the progressive incorporation of Cr into the pargasite structure ($^{[6]}Cr^{3+} = 0.615$ Å, $^{[6]}Al^{3+} = 0.535$ Å; Shannon 1976). The cell volume

TABLE 1. Synthesis conditions and parageneses obtained

Nominal X_{Cr}	T ($\pm$ 10 °C)	P ($\pm$ 50 bar)	Pt-tube loading	Duration (hours)	Parageneses
0.0	900	3000	Gel + 15 wt% water	72	Al-pargasite + ((Mg-diopside))
0.2	900	3000	Gel + 15 wt% water	72	Al-Cr-pargasite + ((Mg-Cr-diopside))
0.4	900	3000	Gel + 15 wt% water	72	Al-Cr-pargasite + (Mg-Cr-diopside)
0.6	900	3000	Gel + 15 wt% water	72	Al-Cr-pargasite + (Mg-Cr-diopside)
0.8	900	3000	Gel + 15 wt% water	72	Al-Cr-pargasite + Mg-Cr-diopside
1.0	900	3000	Gel + 15 wt% water	72	Al-Cr-pargasite + Mg-Cr-diopside
0.0	900	3000	Gel + 15 wt% NaCl 1 M	72	Al-pargasite + ((Mg-diopside))
0.0	900	3000	Gel + 15 wt% NaCl 2 M	72	Al-pargasite + ((Mg-diopside))
0.0	900	3000	Gel + 15 wt% NaCl 4 M	72	Al-pargasite + ((Mg-diopside))
0.2	900	3000	Gel + 15 wt% water // Cr^0	72	Al-Cr-pargasite + ((Mg-Cr-diopside)) // eskolaite
0.4	900	3000	Gel + 15 wt% water // Cr^0	72	Al-Cr-pargasite + (Mg-Cr-diopside) // eskolaite
0.6	900	3000	Gel + 15 wt% water // Cr^0	72	Al-Cr-pargasite + Mg-Cr-diopside // eskolaite
0.8	900	3000	Gel + 15 wt% water // Cr^0	72	Al-Cr-pargasite + Mg-Cr-diopside // eskolaite
1.0	900	3000	Gel + 15 wt% water // Cr^0	72	Al-Cr-pargasite + Mg-Cr-diopside // eskolaite
1.0	900	20000	Gel + 18 wt% water	7	Al-Cr-pargasite + Mg-Cr-diopside

Note: $X_{Cr} = {}^{[6]}Cr / {}^{[6]}(Cr + Al)$; ( ) Minor phase; (( )) Trace; // Pt-foil partition.

TABLE 2. Fractions of Na and Cr in the residual fluids (mol% and atomic fraction) for syntheses without metal Cr as a function of the nominal Cr content

Nominal X_{Cr}	Na, mol%	Cr, mol%	Na / Cr
0.2	17.0	45.5	1.89
0.4	20.5	40.3	1.31
1.0	30.5	33.0	0.94

TABLE 3. Unit-cell parameters for pargasites along the Al-Cr join (900 °C, 3 kbar; experiments without Cr metal

Nominal X_{Cr}	a (Å)	b (Å)	c (Å)	β (°)	V (Å³)
0.0	9.889(2)	17.948(9)	5.279(1)	105.50(1)	902.9
0.2	9.884(8)	17.96(3)	5.277(1)	105.45(2)	902.9
0.4	9.877(5)	17.96(3)	5.281(1)	105.44(4)	903.0
0.6	9.877(2)	17.966(8)	5.282(1)	105.43(1)	903.5
0.8	9.871(4)	17.97(1)	5.285(1)	105.38(1)	903.9
1.0	9.865(2)	17.971(9)	5.283(1)	105.33(1)	903.3

Note: X_{Cr} = [6]Cr / [6](Cr + Al).

V increases in agreement with the increase of b.

EMP. Pyroxene grains are blocky and generally more than 8 μm in size. The average composition derived from six representative analyses of the diopside obtained for nominal X_{Cr} = 0.6 is given in Table 5. The corresponding average structural formula, calculated on the basis of six O atoms, is: $(Ca_{0.88}Na_{0.07}Mg_{0.05})(Mg_{0.72}Cr_{0.06}Al_{0.22})(Si_{1.77}Al_{0.23})O_6$. The actual X_{Cr} value of the Cr-diopside is approximately 0.21.

Amphibole grains are elongated; their dimensions can reach 10 μm in length and about 3 μm in width. For nominal $X_{Cr} \le$ 0.4, amphiboles cannot be analyzed with the EMP due to their small grain size. However, owing to the absence of significant amounts of accessory phases, and to the absence of Cr^{6+} in the fluid phase, we assign the actual X_{Cr} values of these amphiboles to the nominal X_{Cr} values.

For higher X_{Cr} values, two amphiboles, corresponding to nominal X_{Cr} = 0.6 and 1, could be analyzed with the EMP. Average compositions derived from, respectively, 8 and 11 representative EMP analyses are given in Table 5. The resulting

FIGURE 1. A schematic drawing of (**a**) the standard setup and (**b**) the double-chamber tube setup used for (chromium)-pargasite synthesis.

structural formulae, calculated on the basis of $O_{22}(OH)_2$, are as follows:

$Na_{0.89}(Ca_{1.83}Na_{0.17})(Mg_{3.90}Al_{0.67}Cr_{0.43})(Si_{6.19}Al_{1.81})O_{22}(OH)_2$, nominal X_{Cr} = 0.6, actual X_{Cr} = 0.39,

$Na_{0.93}(Ca_{1.83}Na_{0.17})(Mg_{3.88}Al_{0.63}Cr_{0.42})(Si_{6.31}Al_{1.69})O_{22}(OH)_2$, nominal X_{Cr} = 1.0, actual X_{Cr} = 0.40.

The present results show that the upper limit for Cr incorporation in pargasite is 0.43 ± 0.06 apfu (Table 5), at least under the experimental conditions applied. The nominal X_{Cr} values will be used in the following discussion of the XRD and FTIR results.

The (chromium)-pargasites obtained are multi-component solid solutions. Compared with the ideal pargasite structural formula: $NaCa_2(Mg_4M^{3+})(Si_6Al_2)O_{22}(OH)_2$, there is an excess of Si at tetrahedral sites, and an excess of M^{3+} (Al^{3+} + Cr^{3+}) at the M1,2,3 sites. The resultant cation charge excess is balanced almost exactly by the incorporation of some Na^+ at the M4 site (replacing Ca^{2+}) and by a deficit of Na^+ at the A-site. Therefore, our synthetic amphiboles can be considered as a quaternary solid solution involving: pargasite-$NaCa_2(Mg_4M^{3+})(Si_6Al_2)O_{22}(OH)_2$, tremolite-$Ca_2Mg_5Si_8O_{22}(OH)_2$, richterite-$Na(NaCa)Mg_5Si_8O_{22}(OH)_2$, and tschermakite-$Ca_2(Mg_3Al_2)(Si_6Al_2)O_{22}(OH)_2$.

FTIR spectrometry in the OH-stretching region. Infrared spectra of amphiboles in the 3800–3500 cm^{-1} region are sensitive to the cation occupancies of the M3 and the two M1 sites (e.g., Hawthorne 1983). For the more-disordered (aluminum)-pargasite end-member, as inferred from previous work on synthetic pargasites (Raudsepp et al. 1987; Welch et al. 1994; Robert et al. 1996), the M1 sites are occupied solely by Mg, the M2 site occupancy is 1.5 Mg + 0.5 Al, and the M3 site occupancy is 0.5 Mg + 0.5 Al. In such a case, 50% of OH groups are adjacent to 3 Mg and 50% to 2 Mg and 1 Al. So, two OH-stretching bands are expected: a high-wavenumber one due to OH groups adjacent to Mg_3 and a lower-wavenumber one assigned to OH groups adjacent to Mg_2Al. These two bands are effectively observed at 3714 and 3681 cm^{-1}, respectively. However, a third band is present at 3656 cm^{-1} (Fig. 2). This band can be assigned to OH groups pointing toward vacant A-sites (Raudsepp et al. 1987; Della Ventura et al. 1999). The wavenumber shift between the (Mg_3)-OH → Na and the (Mg_2Al)-OH → Na bands is the same as that recorded by Semet (1973) in a synthetic magnesiohastingsite.

For the Cr-saturated pargasite (nominal X_{Cr} = 1, actual $X_{Cr} \approx$ 0.4), four OH-stretching bands are clearly observed (Fig. 3): the same two intense bands already observed for Cr-free pargasite, another intense band at 3660 cm^{-1} and a small one at 3639 cm^{-1}. The 3660 cm^{-1} band is assigned to OH groups adjacent to Mg_2Cr.
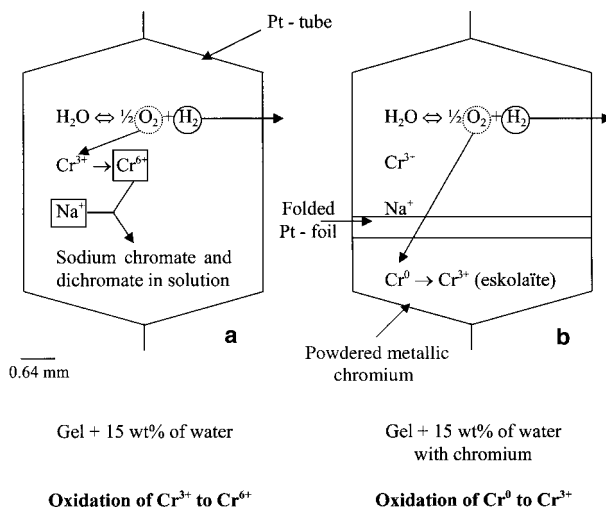
TABLE 4. Unit-cell parameters for pargasites along the Al-Cr join (900 °C, 3 kbar; experiments with Cr metal)

Nominal X_{Cr}	a (Å)	b (Å)	c (Å)	β (°)	V (Å³)
0.0	9.889(2)	17.948(9)	5.279(1)	105.50(1)	902.9
0.2	9.898(3)	17.96(1)	5.286(1)	105.54(1)	905.3
0.4	9.892(2)	17.95(1)	5.284(1)	105.46(1)	904.3
0.6	9.890(2)	17.97(1)	5.283(1)	105.48(2)	904.9
0.8	9.892(5)	18.00(2)	5.280(1)	105.51(2)	905.9
1.0	9.910(7)	17.98(3)	5.281(1)	105.51(3)	906.7

Note: X_{Cr} = [6]Cr / [6](Cr + Al).

TABLE 5. Average compositions of pyroxene and amphibole minerals as determined by electron microprobe analysis of dehydroxylated samples synthesized at 900 °C and 3 kbar with metal chromium for nominal X_{Cr} = 0.6 and 1.0

	Diopside	Pargasite	Pargasite
Nominal X_{Cr}	0.6	0.6	1.0
Number of analyses	6	8	11
Composition (wt%)			
SiO_2	49.10(0.91)	42.03(0.75)	43.05(0.54)
Al_2O_3	10.66(1.27)	14.28(0.29)	13.44(0.46)
Cr_2O_3	2.18(0.29)	3.70(0.29)	3.66(0.51)
MgO	14.39(0.64)	17.78(0.39)	17.78(0.27)
CaO	22.69(0.64)	11.57(0.13)	11.68(0.23)
Na_2O	0.98(0.18)	3.73(0.16)	3.86(0.09)
Total	100.00	93.09	93.47
Formula proportions of cations			
Calculation basis	O_6	$O_{22}(OH)_2$	$O_{22}(OH)_2$
Si	1.77(0.03)	6.19(0.04)	6.31(0.04)
Al	0.45(0.05)	2.48(0.04)	2.32(0.07)
Cr	0.06(0.01)	0.43(0.03)	0.42(0.06)
Mg	0.77(0.03)	3.90(0.04)	3.88(0.06)
Ca	0.88(0.02)	1.83(0.04)	1.83(0.04)
Na	0.07(0.01)	1.06(0.04)	1.10(0.03)

Notes: The numbers in parentheses are errors associated with the analyses and represent two standard deviations of the microprobe analyses.

The –21 cm^{-1} OH-stretching band shift, produced by the replacement of Al by Cr, is typical of the introduction of a transition element in the neighborhood of an OH group (Della Ventura et al. 1996, 1997; Semet 1973). The 3639 cm^{-1} band can be assigned to OH groups bonded to Mg_2Cr and pointing toward a vacant A-site. It corresponds to the previously observed 3656 cm^{-1} band, assigned to the (Mg_2Al)-OH $\rightarrow$ [A]□ association, shifted toward lower wavenumbers. The presence of a 3656 cm^{-1} band is probable, but the intense 3660 cm^{-1} band prevents its observation.

Along the Al-Cr join (Fig. 4), we can observe progressive variations in the intensities of each infrared band. Table 6 gives the relative areas of OH-stretching absorption bands assigned to the different 2M1M3 environments (i.e., Mg_3, Mg_2Al, and Mg_2Cr) facing a filled A-site, and of the low-wavenumber band assigned to OH-groups pointing toward vacant A-sites. Several observations deserve comments:

(1) Along the Al-Cr join, a band assigned to OH groups pointing toward vacant A-sites is always observed : at 3656 cm^{-1} for X_{Cr} = 0 and at 3639 cm^{-1} for X_{Cr} > 0. Its relative intensity does not vary significantly with X_{Cr} (Fig. 4 and Table 6). The proportion of OH groups facing a vacant A-site can be deduced from the measurement of relative band intensities. However, it is known that the molar absorptivities for the stretching absorption band of an OH-group pointing toward a vacant A-site is 2.2 times larger than that of an OH-group pointing toward a filled A-site (Hawthorne et al. 1997). Applying this correction coefficient we can conclude that the proportion of A-site vacancies is constant within experimental errors along the Al-Cr pargasite join (Table 6). The proportion of vacant A-sites deduced from FTIR data (less than 3%) is significantly less than that derived from EMP measurements (close to 10%). This discrepancy is due to the fact that only those OH-groups adjacent to Mg_2Cr and pointing toward an A-site vacancy can be identified in the complex FTIR spectra of Cr-bearing pargasite (3639 cm^{-1} band). The 3656 cm^{-1} band, corresponding to the (Mg_2Al)-OH $\rightarrow$ [A]□ association, which must remain present with a non negligible intensity, is overlapped by the
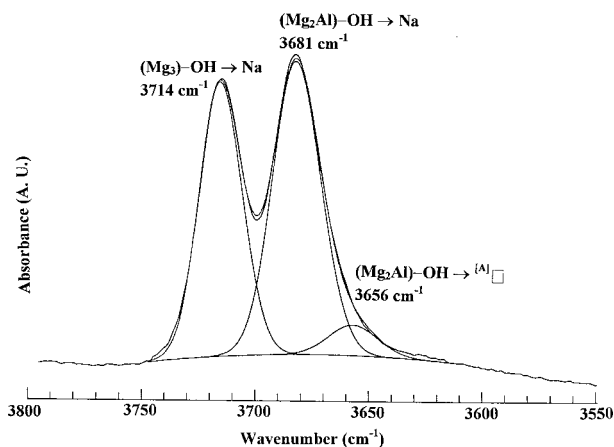
FIGURE 2. FTIR OH-stretching region spectra of (aluminum)-pargasite (nominal X_{Cr} = 0), synthesized at 900 °C and 3 kbar.

3660 cm^{-1} band. The proportion of A-site vacancies is therefore significantly underestimated from FTIR data.

(2) The proportion of Mg_2M^{3+} environments (Table 6) is significantly greater than 50%, namely around 56% for the (aluminum)-pargasite end-member, and around 60% for the Cr-bearing pargasites. This observation is in agreement with EMP data, which have also shown an excess of [6]M^{3+} compared with the theoretical stoichiometry, and with the probable persistence of the 3656 cm^{-1} band, overlapped by the Cr-related 3660 cm^{-1} one.

(3) Considering that M1 sites are occupied only by Mg in pargasites (Oberti et al. 1995), the relative area of the (Mg_3)-OH, (Mg_2Al)-OH and (Mg_2Cr)-OH infrared bands give, respectively, the proportion of Mg, Al, and Cr present in the M3 sites. Figure 5 shows the cation occupancy of M3 sites as a function of the nominal X_{Cr} value. We can observe significant modifications along the Al-Cr join: (1) the sum of the relative areas of the (Mg_2Cr)-OH bands (3660 and 3639 cm^{-1}) regularly increases
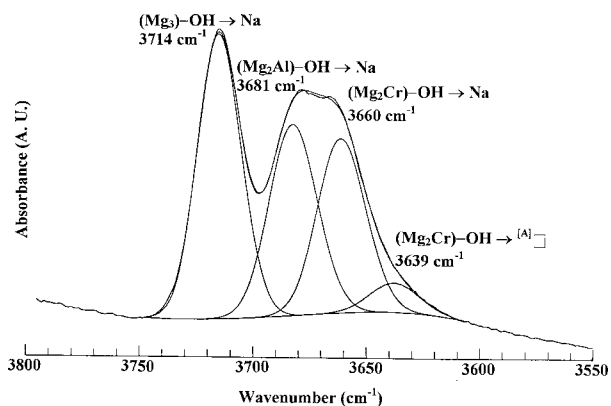
FIGURE 3. FTIR OH-stretching region spectra of (chromium)-pargasite (nominal X_{Cr} = 1), synthesized at 900 °C and 3 kbar with Cr metal.
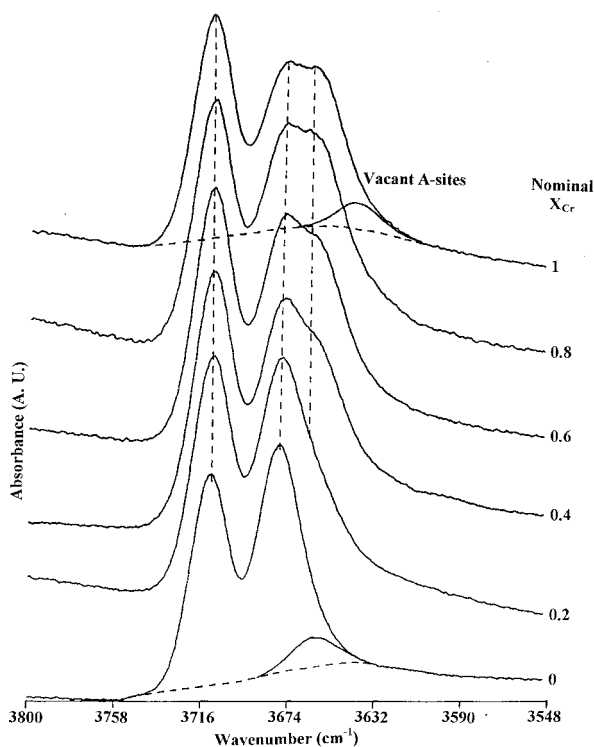
FIGURE 4. Evolution of the FTIR OH-stretching region spectra of pargasite, synthesized at 900 °C and 3 kbar with Cr metal, as a function of nominal X_{Cr}.

TABLE 6. Relative areas of OH-stretching bands corresponding to OH groups bonded to Mg_3, Mg_2Al, or Mg_2Cr facing a filled A-site along the Al-Cr join (900 °C, 3 kbar; experiments with metallic Cr); raw and corrected relative area of OH groups facing vacancies

Nominal X_{Cr}	Mg_3	Mg_2Al	Mg_2Cr	Mg_2M^{3+}	A vacancies (raw)	A vacancies (corrected)
0.0	42	56	0	56	5	2.3
0.2	40	44	15	59	3	1.4
0.4	39	37	22	59	4	1.8
0.6	36	37	25	62	5	2.3
0.8	36	35	26	61	6	2.7
1.0	38	34	26	60	5	2.3

TABLE 7. Possible octahedral site occupancies of the (chromium)-pargasite synthesized at 900 °C and 3 kbar with metal chromium for nominal $X_{Cr} = 0.6$ (actual $X_{Cr} \approx 0.4$)

Sites	Multiplicity	Mg	Al	Cr
M1	2	1	0	0
M3	1	0.36	0.37	0.27
M2	2	0.77	0.15	0.08
Total		3.90	0.67	0.43

(1995), who have shown that in a pargasite from an ultramafic environment, up to 0.32 Al apfu enters the M3 site, and that there is a distribution of Al over M2 and M3 sites. In contrast, although natural pargasites studied by Oberti et al. (1995) contained up to 0.21 Cr apfu, they did not seem to incorporate Cr at the M3 site. However, in natural systems the presence of Fe and Ti, partial dehydrogenation, and a significant cummingtonite component strongly affect site geometry, and thus cation incorporation and ordering.

A-site vacancies

In all the synthetic pargasites of this work, we have observed the presence of vacant A-sites. For nominal $X_{Cr} = 0.6$ and 1.0, EMP analyses revealed that residual Na is all incorporated into the M4 sites as the amount of $^ANa + ^{M4}Na$ is the expected value (1 apfu). For $X_{Cr} = 0$, no variation in the intensity
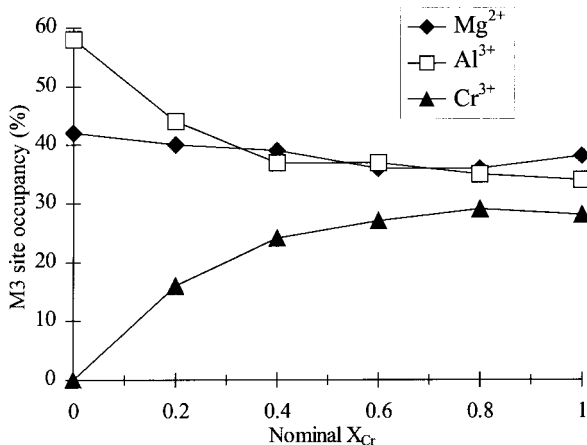
with the Cr content, characterizing the progressive incorporation of Cr^{3+} in M3 sites; (2) the chromium saturation is reached for a X_{Cr} value close to 0.4, as previously observed from EMP analyses; (3) the relative area of the (Mg_2Al)-OH band (3681 cm^{-1}) decreases in response to the replacement of $^{[6]}Al$ by $^{[6]}Cr$; (4) the (Mg_2Al)-OH band never disappears, indicating that a significant amount of $^{[6]}Al$ remains present, which provides further confirmation of the instability of the theoretical (chromium)-pargasite end-member; and (5) the amount of $^{[6]}M^{3+}$ (Al^{3+} and Cr^{3+}) is systematically greater than the expected proportion, that is to say, 1 M^{3+} per 5 M1,2,3 sites, predicted by the theoretical formula.

For $X_{Cr} = 0.6$ we deduced from EMP analyses that the 5 M1,2,3 sites are occupied by 3.90 Mg + 0.67 Al + 0.43 Cr. Using the hypothesis that the M1 sites are occupied only by Mg we obtained the M3 site occupancy from FTIR data. Combining EMP and FTIR results, we can deduce the possible M1,2,3 site occupancies of (chromium)-pargasite for nominal $X_{Cr} = 0.6$ (actual $X_{Cr} \approx 0.4$) (Table 7). We can note that Cr^{3+} has an higher preference for octahedra adjacent to OH groups than does Al. This situation is classical in polysite minerals, as the transition element systematically favors chemically anisotropic sites (O, OH) (Robert and Gaspérin 1985; Della Ventura et al. 1993, 1998). Aluminium is distributed between the M2 and M3 sites. Our results for Al are in agreement with Oberti et al.

FIGURE 5. Pargasite M3 site occupancy as a function of the nominal X_{Cr} values along the Al-Cr join (900 °C, 3 kbar; experiments with Cr metal).

of the $(Mg_2Al)-OH \rightarrow$ [A]□ infrared band was observed for pargasites synthesized with increasingly concentrated NaCl solutions (1 to 4 M). Thus, it seem that for whatever X_{Cr} (from 0 to 1.0), A-site vacancies of synthetic pargasites are controlled by crystal-chemical constraints, as in many A-site occupied clinoamphiboles, rather than by Na solubilization into the hydrothermal solution.

Effect of pressure

The results of this work were confirmed at 900 °C and 20 kbar, showing that increasing pressure does not change the mechanisms of Cr incorporation in pargasite.

GEOLOGICAL APPLICATIONS

The maximum Cr content in pargasites observed in this experimental work, at 900 °C and 3 kbar, closely corresponds to the maximum Cr solubility (0.42 apfu) observed in naturally occurring Cr-bearing pargasites from the Oman ophiolitic complex, as analyzed by Augé (personal communication, 1996). This similarity, and the fact that the upper solubility limit of Cr remains constant for $0.4 \leq X_{Cr} \leq 1$ in the bulk system, suggests that the maximum Cr content of pargasite is not controlled by the Cr activity in the system but by crystal-chemical constraints. In addition, this similarity is an argument in favor of the genesis of (chromium)-pargasites included in ophiolitic chromitites at temperatures significantly lower than the liquidus temperature of the mafic melt. The common association of these (chromium)-pargasites with another hydrous phase, Na-phlogopite, corroborates this conclusion, since the upper thermal stability limit of these micas is around 1000 °C, at $P \leq 5$ kbar (Carman 1974; Liu 1989). So, the origin of ophiolitic (chromium)-pargasite is likely due to metasomatic processes affecting the upper mantle.

This study has also shown that, under hydrothermal conditions, a large part of the Cr can be oxidized and solubilized in the fluid phase as chromate and/or dichromate. This raises the general problem of Cr transportation by hydrothermal fluids. Possible remedies in experimental studies are the extraction of Cr^{6+} by a fluid phase under oxidizing conditions, or its precipitation, or incorporation in solid phases under reducing ones.

ACKNOWLEDGMENTS

REFERENCES CITED

Appleman, D.E. and Evans, H.T. (1973) Job 9214: Indexing and least-square refinement of powder diffraction data. U.S. National Technical Information Service, Document PB 216–188.
Carman, J.H. (1974) Synthetic sodium phlogopite and its two hydrates: stabilities, properties and mineralogic implications. American Mineralogist, 59, 261-273.
Deer, W.A., Howie, R.A., and Zussman, J. (1992) An introduction to the rock-forming minerals, 2nd ed., 696 p. Longman scientific and technical, Harlow, U.K.

Della Ventura, G., Robert, J.-L., Raudsepp, M., and Hawthorne, F.C. (1993) Site occupancies in monoclinic amphiboles: Rietveld structure refinement of synthetic nickel magnesium cobalt potassium richterite. American Mineralogist, 78, 633-640.
Della Ventura, G., Robert, J.-L., and Hawthorne, F.C. (1996) Infrared spectroscopy of synthetic (Ni, Mg, Co)-potassium-richterite. In M.D. Dyar, C. McCammon, and M.W. Schaefer, Eds., Mineral spectroscopy: A Tribute to Roger G. Burns, p. 55-63. The Geochemical Society, St. Louis, Missouri.
Della Ventura, G., Robert, J.-L., Raudsepp, M., Hawthorne, F.C., and Welch, M.D. (1997) Site occupancies in synthetic monoclinic amphiboles: Rietveld structure refinement and infrared spectroscopy of (nickel, magnesium, cobalt)-richterite. American Mineralogist, 82, 291–301.
Della Ventura, G., Robert, J.-L., Hawthorne, F.C., Raudsepp, M., and Welch, M.F. (1998) Contrasting patterns of [6]Al order in synthetic pargasite and Co-substituted pargasite. Canadian Mineralogist, 36, 1237–1244.
Della Ventura, G., Hawthorne, F.C., Robert, J.-L., Delbove, F., Welch, M.D., and Raudsepp, M. (1999) Short-range order of cations in synthetic amphiboles along the richterite-pargasite join. European Journal of Mineralogy, 11, 79–94.
Garvey, R. (1987) Least squares unit cell refinement, version 86.2. Department of Chemistry, North Dakota State University.
Guédon, C.-I. (1996) Cristallochimie des pargasites chromifères de synthèse, 39 p. DEA, University of Orléans, France.
Hamilton, D.L. and Henderson, C.M.B. (1968) The preparation of silicate compositions by a gelling method. Mineralogical Magazine, 36, 832–838.
Hawthorne, F.C. (1983) Quantitative characterization of site-occupancies in minerals. American Mineralogist, 68, 287–306.
Hawthorne, F.C., Della Ventura, G., Robert, J.-L., Welch, M.D., Raudsepp, M., and Jenkins, D.M. (1997) A Rietveld and infrared study of synthetic amphiboles along the potassium-richterite-tremolite join. American Mineralogist, 82, 708–716.
Johan, Z., Dunlop, H., LeBel, L., Robert, J.-L., and Volfinger, M. (1983) Origin of chromite deposits in ophiolitic complexes: evidence for a volatile and sodium-rich fluid phase. Fortschritte der Mineralogie, 61, 105–107.
Liu, X.F. (1989) Signification pétrogénétique des micas trioctaédriques sodiques: modélisation expérimentale dans le système Na2O-K2O-MgO-Al2O3-SiO2-H2O-(TiO2-HF-D2O), 105 p. Ph.D. dissertation, University of Orléans, France.
Oberti, R., Hawthorne, F.C., Ungaretti, L., and Cannillo, E. (1995) [6]Al disorder in amphiboles from mantle peridotites. Canadian Mineralogist, 33, 867–878.
Papin, A., Sergent, J., and Robert, J.-L. (1997) Intersite OH-F distribution in an Al-rich synthetic phlogopite. European Journal of Mineralogy, 9, 501–508.
Raudsepp, M., Turnock, A., Hawthorne, F.C., Sheriff, B., and Hartman, J.S. (1987) Characterization of synthetic pargasitic amphiboles $NaCa_2Mg_4M^{3+}Si_6Al_2O_{22}(OH,F)_2$; M^{3+} = Al, Cr, Ga, Sc, In) by infrared spectroscopy, Rietveld structure refinement and ^{27}Al, ^{29}Si, and ^{19}F MAS-NMR spectroscopy. American Mineralogist, 72, 580–593.
Robert, J.-L. and Gaspérin, M. (1985) Crystal Structure Refinement of Hendricksite, a Zn- and Mn-rich Trioctahedral Potassium Mica: Contribution to the Crystal Chemistry of Zinc-Bearing Minerals. Tschermaks Mineralogische und Petrologische Mitteilungen, 34, 1–14.
Robert, J.-L., Della Ventura, G., and Hawthorne, F.C. (1996) Infrared characterization of (OH,F)-pargasites. Physics Chemistry of Minerals, 23, 4/5, 307.
Roux, J. and Volfinger, M. (1996) Mesures précises à l'aide d'un détecteur courbe. Journal de Physique, C4, 127–134.
Semet, M.P. (1973) A crystal-chemical study of synthetic magnesiohastingite. American Mineralogist, 58, 480–494.
Shannon, R.D. (1976) Revised effective ionic radii and systematic studies of interatomic distances in halides and chalcogenides. Acta Crystallographica, A32, 751–767.
Strens, R.G.J. (1974) The common chain, ribbon, and ring silicates. In V.C. Farmer, Ed., The infrared spectra of minerals. Mineralogical Society, London, U.K.
Veblen, D.R. and Ribbe, P.H. (1982) Amphiboles: Petrology and experimental phase, 390 p. Mineralogical Society of America Reviews in Mineralogy, 9B.
Welch, M.D., Kolodziejski, W., and Klinowski, J. (1994) A multinuclear NMR study of synthetic pargasite. American Mineralogist, 79, 261–268.